J. Fluid Mech. (1995), *vol.* 295, *pp.* 305–335

LDA measurements in the near-wall region of a turbulent pipe flow

By F. DURST, J. JOVANOVIĆ AND J. SENDER

Lehrstuhl für Strömungsmechanik, Universität Erlangen-Nürnberg, Cauerstrasse 4, D-91058 Erlangen, Germany.

(Received 22 July 1993 and in revised form 8 March 1995)

This paper presents laser-Doppler measurements of the mean velocity and statistical moments of turbulent velocity fluctuations in the near-wall region of a fully developed pipe flow at low Reynolds numbers. A refractive-index-matched fluid was used in a Duran-glass test section to permit access to the near-wall region without distortion of the laser beams. All measurements were corrected for the influence of the finite size of measuring control volume. Measurements of long-time statistical averages of all three fluctuating velocity components in the near-wall region are presented. It is shown that the turbulence intensities in the wall region do not scale with inner variables. However, the limiting behaviour of the intensity components very close to the wall show only small variations with the Reynolds number. Measurements of higher-order statistical moments, the skewness and flatness factors, of axial and tangential velocity components confirm the limiting behaviour of these quantities obtained from direct numerical simulations of turbulent channel flow. The comparison of measured data with those obtained from direct numerical simulations reveals that noticeable discrepancies exist between them only with regard to the flatness factor of the radial velocity component near the wall. The measured v' flatness factor does not show the steep rise close to the wall indicated by numerical simulations. Analysis of the measured data in the near-wall region reveals significant discrepancies between the present LDA measurements and experimental results obtained using the hot-wire anemometry.

1. Introduction

Over the past three decades, turbulent wall shear flows have been the target of numerous experimental and lately also numerical investigations. These studies have provided information on the mean flow field and turbulence intensities for the wall boundary layer, pipe and channel flows. All of this work has resulted in general agreement regarding the flow structure away from the wall. Close to the wall, however, questions regarding the turbulence properties still remain, since the experimental data are inconsistent and in some details contradict the results obtained from direct numerical simulations (see Kim, Moin & Moser 1987 and Lyons, Hanratty & McLaughlin 1991). This evidence suggests that more refined experimental work is needed in the near-wall region of turbulent boundary layers, pipe and channel flows.

Currently, there is considerable interest in the structure of turbulent boundary layers. This interest has an engineering relevance, since turbulence in the wall region has a direct influence on the viscous drag and heat-transfer processes. A great deal

of work has been done to provide detailed information of the properties of near-wall turbulence, but data were obtained with only partial success. Owing to the small thickness of the viscous sublayer, most measuring techniques used so far failed to satisfy the space and/or time resolution requirements imposed by the flow structure. For this reason, well-documented and self-consistent quantitative data are not yet available that reliably describe all turbulence properties in the region very close to the wall.

The objective of this paper is to present new experimental data on the mean velocity and turbulence statistics in the near-wall region using state-of-the-art laser-Doppler (LDA) techniques. Well-designed LDA systems allow experimental data to be obtained with a much greater degree of confidence than previously, when experimental investigations had to rely entirely on hot-wire anemometry measurements. Hot-wire techniques work very reliably away from the walls, but in the present study, emphasis is placed on the region of the viscous sublayer and the buffer region of wall-bounded flows. In these regions, invasive measuring techniques result in problems of applicability. The disturbance of the flow yields the scatter of the existing experimental data known from the literature. For invasive measuring techniques, the deviations are largest in the immediate vicinity of the walls. The results to be presented support this conjecture.

To explore the near-wall region experimentally, the application of optical measuring techniques is preferable owing to the severe spatial resolution demands enforced by the special nature of the flow. Advanced laser-Doppler anemometers can be designed to satisfy these demands and, therefore, are the most suitable techniques for sublayer measurements, particularly in liquid flows. However, the application of this technique requires a well designed test rig to avoid deflections of light beams near the solid surface. For pipe flow investigations, refractive-index-matched fluids can be used to eliminate influences of the cylindrical pipe walls on the laser beams. A specially designed test rig was used in the present study to meet these requirements. Details of the experimental facility are described in § 2 together with the instrumentation used for turbulence measurements.

To obtain accurate laser-Doppler measurements, it is important to consider the influence of the finite size of the measuring control volume. Time-averaged turbulence properties show a dependence on the measuring volume size and require the application of volume corrections. The appropriate corrections can be derived analytically to account for the effects mentioned above. The procedure for correcting laser-Doppler measurements taken in flow regions with high velocity gradients is summarized in § 3. This procedure was applied at each measuring position in the flow to yield reliable turbulence data in the near-wall region.

Additional efforts were necessary in order to minimize the influence of electronic noise on the measured data and to account for the small angle misalignment of the optical system with respect to the flow. The influence of these factors turned out to be small in absolute terms, but became more significant in the near-wall region where the mean velocity and turbulence intensities approach zero at the solid surface. As the present paper shows, the application of corrections is the basis for good turbulence measurements up to the wall.

The experimental results are presented in § 4. These measurements include distributions of the mean velocities, turbulence intensities, as well as higher-order moments of the axial, radial and tangential velocity components. The experimental data demonstrate the importance of the gradient-broadening corrections used for laser-Doppler measurements near the walls. The results obtained are compared with data from ex-

perimental investigations and direct numerical simulations available in the literature. Detailed comparison of the limiting behaviour of turbulence quantities near the wall indicate important differences between the present LDA measurements and existing hot-wire results. It appears that hot-wire anemometry is not a very convenient technique for turbulence measurements in the viscous sublayer. Some of the questions regarding the behaviour of turbulence intensities in the near-wall region are clarified but some still remain. These remaining questions are pointed out in the paper and suggestions are made for utilizing combined experimental and numerical studies to provide final answers.

2. Test section and instrumentation

2.1. *Test section*

To carry out detailed and reliable near-wall velocity measurements, a special test section was designed and built. Its major parts are shown schematically in figure 1. It consisted of a closed-loop pipe flow installation driven by a screw conveyor pump operating in suction mode. This screw conveyor pump was chosen because of its very low flow-rate pulsations. Electronic control of the pump was available which allowed flow-rate settings between 0.6 and 20 $m^3 h^{-1}$, with a tolerance of 1% of the prescribed value. As figure 1 shows, the flow was supplied from a large settling tank to the working section that was located about 4 m downstream, providing a development length of about 80 pipe diameters. In addition, the flow was tripped at the inlet of the pipe to enhance the turbulence and, in this way, to reduce the development length of the flow. Using the highest flow rate, a maximum Reynolds number (based on a pipe diameter and the bulk velocity) of $Re = 30\,000$ could be achieved with a pipe diameter of $D = 50$ mm. The measurements presented here were performed mainly at a low Reynolds number, $Re = 7442$, corresponding to a bulk velocity of $\overline{U}_B = 0.64\,m\,s^{-1}$. Additional measurements were also made at slightly higher Reynolds numbers, $Re = 13\,500$ and 20 800, corresponding to bulk velocities of 1.16 and 1.79 $m\,s^{-1}$, respectively.

In order to permit laser-Doppler measurements, the test section was made from a Duran-50 glass pipe. This pipe was centrally mounted in a viewing box as indicated in figure 1. To avoid any interference of the pipe with the light beams, the test fluid was selected to be refractive-index-matched to the Duran glass, the material of the pipe wall. To achieve precise matching of refractive indices, two Diesel oils of slightly different refractive indices were selected and mixed in such a way that the refractive index of the glass pipe was achieved. In addition, the temperature of the test fluid was controlled by heating and cooling elements installed in the downstream settling chamber of the test rig. The same liquid also passed through the square viewing box mounted around the test section. In this way, the temperature controller permitted thermal effects on the refractive index of the test fluid to be kept within $\pm 5 \times 10^{-4}$. This was found to be sufficient to ensure undisturbed velocity measurements close to the pipe walls.

The kinematic viscosity of the working fluid was measured with a commercial viscosimeter. The value obtained for the working temperature of 20°C, $\nu = 4.3 \times 10^{-6}\ m^2\,s^{-1}$, was found to be constant and independent of the shear rate, i.e. the fluid showed Newtonian properties.

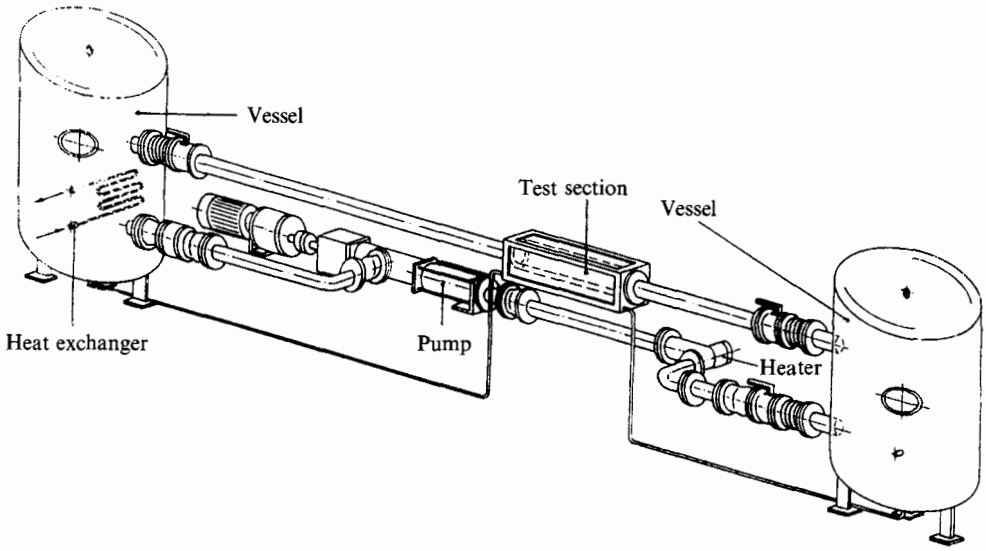

FIGURE 1. Closed-loop pipe flow test section.

2.2. *Instrumentation*

A special laser-Doppler optical system was designed for the present measurements. This system is shown schematically in figure 2, where its major parts and also its arrangement with the respect to the test section are shown. The system operates with a 30 mW helium-neon laser and double Bragg cell transmission optics. The Bragg cells were driven with 40 and 41.7 MHz, giving a shift frequency of 1.7 MHz. For the sublayer measurements the Bragg cells were driven with 40 and 40.2 MHz, giving a shift frequency of 200 kHz.

The optical arrangement was laid out to yield a measuring control volume, based on the e^{-2} light intensity cut-off point, of 70 μm in diameter and 250 μm in length. These dimensions were calculated from:

$$d = \frac{4\lambda f}{E\pi d_{beam}\cos(\theta)}, \tag{2.1}$$

and

$$l = \frac{4\lambda f}{E\pi d_{beam}\sin(\theta)}, \tag{2.2}$$

where

λ = laser wavelength,
f = focal length of the transmitting lens,
E = beam expansion factor,
d_{beam} = diameter of unfocused laser beam,
θ = half-intersection angle of the beams.

The calculated dimensions of the measuring control volume were verified by direct measurements using a beam scanner device. A slit of 2 μm width was used to scan the waist of beam, yielding the diameter of the measuring control volume with an estimated accuracy of $\pm 4.5\%$.

Light scattered in the forward direction was collected by the receiving optics and directed onto an appropriately sized pinhole in front of an avalanche photodiode.

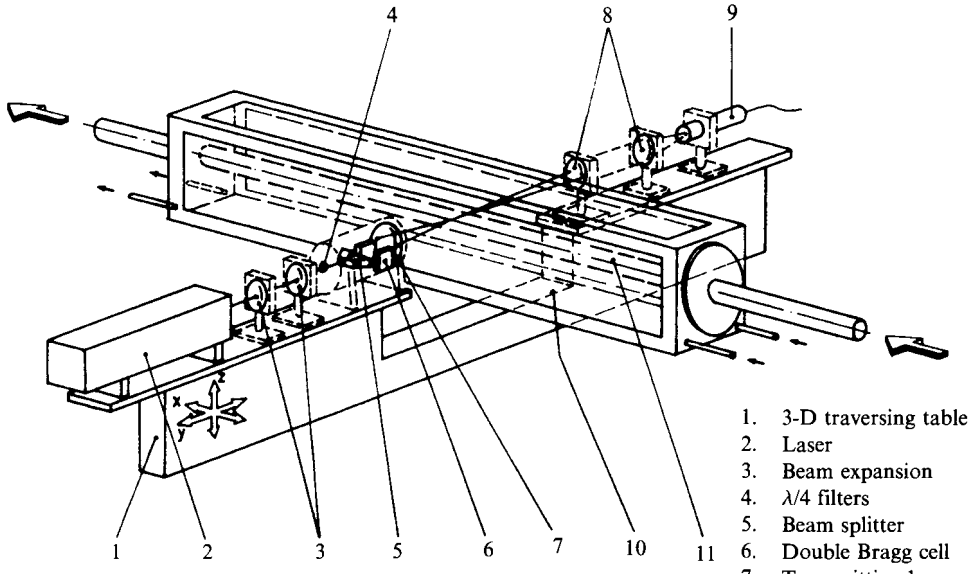

FIGURE 2. Layout of the LDA optical system.

The signal from this diode was bandpass filtered prior to being processed by a LDA counter processor.

The bandpass filter settings in the signal processor were chosen between 100 kHz and 3 MHz to yield a measuring velocity range between 2.6 and $-3.3\,\mathrm{m\,s^{-1}}$. For the data points lying inside the viscous sublayer, the measuring velocity range was between 5.8 and $-0.21\,\mathrm{m\,s^{-1}}$ owing to the decrease in the shift frequency of the Bragg cells.

A TSI Model 1980 counter was used for all of the measurements. Its settings to trigger on LDA signals were controlled in such a way that no signal was obtained when one of the laser beams was blocked. In this way, the influence of noise on the measured data was substantially minimized.

Sufficient particles were present in the oil to measure the turbulent fluctuations. Data rates of 100 Hz were typical for measuring points very close to the wall ($y^+ \approx 0.4$). At locations away from the wall, the average data rate changed in proportion to the local mean velocity. At each measuring location these data rates were smaller than the maximum particle arrival rate (which can be estimated from the flow velocity and the diameter of the measuring control volume) but larger than the Kolmogorov frequency. The Kolmogorov frequency,

$$f_k = \frac{\overline{U}}{2\pi L_k}, \tag{2.3}$$

was estimated from the mean velocity profile and the average dissipation rate, which yielded the lengthscale L_k:

$$L_k = (\nu^3/\bar{\epsilon})^{1/4}. \tag{2.4}$$

The average energy dissipation rate $\bar{\epsilon}$ was obtained from the mean flow parameters per unit mass across the pipe cross-section (see Bakewell & Lumley 1967):

$$\bar{\epsilon} = \frac{\tau_w \pi D L \overline{U}_B}{\rho \pi \frac{1}{4} L D^2} = \frac{4 u_\tau^2 \overline{U}_B}{D}, \tag{2.5}$$

where u_τ is the wall shear velocity to be defined later. For the data to be presented in §4 ($y^+ \geqslant 1$), the data rates correspond to about 20–40 particle arrivals per integral time-scale, which is defined by (4.1). The conditions described above ensured that no more than one particle can be in the measuring control volume and, at the same time, provide a sufficiently high data rate for sampling the velocity fluctuations once per integral timescale of the flow.

The laser-Doppler optical system was placed perpendicular to the measuring test section. The axial velocity component was measured in the vertical plane with a spatial resolution of 70 μm. By rotating the transmitting optics by 90° the radial velocity component was measurable in the vertical plane of the pipe cross-section and the tangential velocity component in the horizontal plane. Hence, the spatial resolution in the tangential direction was limited and prevented measurements closer than ≈ 250 μm to the wall.

To permit detailed flow investigations, a three-dimensional traversing unit was used in such a way that spring loads were applied in all three directions to compensate for the backlashes in the screw drives. Computer-controlled stepping motors were used to traverse the measuring control volume from point to point to yield profile measurements. Comparisons with displacement gauges showed that the positioning repeatability was better than ± 10 μm in all directions. The major inaccuracy in positioning resulted from the zero location of the volume at the wall. To obtain the zero location reliably, the volume was traversed into the wall and the signal due to light scattering by very small particles attached to the wall was recorded at the avalanche photodiode output. The location of the maximum output signal of the photodiode was recorded and taken as the zero position of the volume from the wall. Four to five repeated readings were taken to assure that a high repeatability of the zero location was obtained prior to starting the measurements.

The flow in the near-wall region shows local turbulence intensities of 30–40% and a straight arithmetic averaging of counter processor data would lead to significant errors. For the present measurements, the errors in statistical estimations due to the random arrival of particles in the measuring control volume were eliminated using the equal time sampling method. In this method, the computer was set to sample counter processor data at a constant sampling time interval proportional to the integral timescale of the flow. The data were read from the counter during the time period of 200 ns which corresponds to more than 1000 times the Kolmogorov frequency. Owing to the timer-triggered acquisition mode, the assembly of independent realizations permitted application of the ensemble averaging procedure for evaluation of the mean statistical flow quantities.

For all measurements, the time series of the frequency readings from the counter processor were recorded for subsequent signal processing. Some preliminary data were also evaluated on-line with the measurements. This procedure functioned well only for the mean velocities and turbulence intensities. However, if high-order statistical moments are required, single incorrect data lead to significant errors, even for large data sets. The cause of these errors resulted from the electronic characteristics of the bandpass filters used. It is well known that Chebyshev filters respond to bursts of

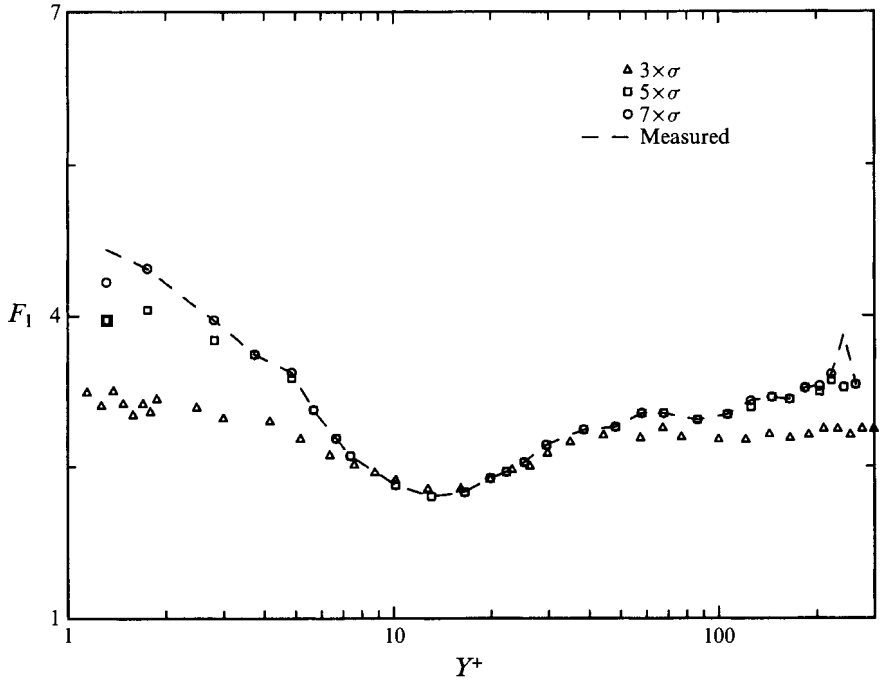

FIGURE 3. Influence of the variable-amplitude cut-off on the measurements of the flatness factor.

large amplitudes with output signals not proportional to the Doppler frequency but to a frequency equal to the upper filter setting. These yielded wrong high-frequency measurements that could be identified in the data, since these samples deviated from the mean velocity by more than ten times the RMS value. These were eliminated from the data set prior to evaluating the final flow properties.

During the experiments, the mean velocity and turbulence intensities were calculated on-line mainly to check the measuring performance. For post-processing of the recorded raw LDA data, the standard deviation measured on-line was taken to limit the range of magnitudes of each individual sample. A range of ± 7 times the RMS value was found to eliminate any spurious data without changing the shape of the probability density distributions. This was verified by repeating the measurements at a few different locations many times since some of these were free from the erroneous signals. In connection with this issue, one may note that the probability density distributions of all three fluctuating velocity components computed from the numerical simulations of turbulent channel flow by J. Kim (1986, personal communication) also corroborate the findings mentioned above.

In figure 3, the distributions of the flatness factor evaluated using limiting ranges of 3, 5 and 7 times the RMS value of the signal are shown. Clearly, the choice of 7 RMS values shows the best cut-off without affecting the shape of profile. Consequently, all data presented in this paper were processed in the manner given above.

3. Applied corrections

3.1. *Finite measuring volume*

In general, the spatial integration of the LDA signals due to the finite size of the measuring control volume affects turbulence measurements. This effect is particularly

important close to the wall since the velocity variations across the measuring volume reach their maximum value in this part of the flow field. In the literature, no unique correction procedure exists to take this influence into account. Recently, Durst *et al.* (1992) (see also Goldstein & Adrian 1971) considered this problem analytically by representing measured mean quantities as averages in time and space:

$$\overline{U}_i = \lim_{T\to\infty} \frac{1}{T} \int_0^T \left\{ \frac{1}{V} \int\int_V \int F U_i \mathrm{d}V \right\} \mathrm{d}t, \tag{3.1}$$

where U_i corresponds to the instantaneous velocity component that depends on time and space coordinates, V is the LDA measuring control volume and the function F accounts for the distribution of the detected particles inside the volume of the integration. Since the detection of a Doppler burst is signal-amplitude triggered, the probability of the detection of a particle is directly proportional to the scattered light intensity. Therefore, for monodisperse particles, the probability of their detection should be identical with the light intensity distribution in the measuring control volume. Hence, owing to the Gaussian light intensity distribution, a higher detectability can be expected in the region near the centre of the measuring control volume.

To facilitate the analytical treatment of (3.1) for signal evaluation, we utilized the following assumptions:

(i) The dominant effect of the spatial integration is assumed to lie only in direction (y) perpendicular to the flow.

(ii) In the measuring volume, the light distribution is similar to the light intensity distribution of the individual laser beams. The detectability function $F(y)$ is proportional to the light intensity in the measuring volume:

$$F(y) = \frac{4}{(2\pi)^{1/2} d} \exp\left[-\frac{1}{2} \left(\frac{y - y_c}{d} \right)^2 \right], \tag{3.2}$$

where d and y_c are the diameter of the measuring control volume (based on the e^{-2} point of the Gaussian light intensity profile) and its distance from the wall, respectively. The diameter of the measuring volume d is defined on the basis of the minimum detectable signal level.

Expressing U_i in the form of a truncated Taylor expansion around the centre of the control volume permitted the derivation of explicit relationships between measured mean values and true local averages.

For the mean velocity and turbulence intensity, the following expressions were obtained for correcting the measured data:

$$\overline{U}_{i\,meas} = \overline{U}_{i\,true} + \frac{d^2}{32} \left(\frac{\mathrm{d}^2 \overline{U}_{i\,true}}{\mathrm{d}y^2} \right) + \cdots, \tag{3.3}$$

$$\overline{u_i^2}_{meas} = \overline{u_i^2}_{true} + \frac{d^2}{16} \left(\frac{\mathrm{d}\overline{U}_{i\,true}}{\mathrm{d}y} \right)^2 + \cdots. \tag{3.4}$$

These results show that the correction for the mean velocity depends on the second derivative of the variation of $\overline{U}_i$ with wall distance, and the correction for the turbulence intensity is proportional to the gradient of the mean velocity. It can also be shown that corrections for the higher-order moments are dependent on the gradient of the mean velocity and the gradient of the lower-order moment. The

expressions derived by Durst *et al.* (1992) are

$$\overline{u_i^3}_{meas} = \overline{u_i^3}_{true} + \frac{3d^2}{16}\left(\frac{d\overline{u_i^2}}{dy}\right)_{true}\left(\frac{d\overline{U}_i}{dy}\right)_{true} + \frac{d^2}{32}\left(\frac{d^2\overline{u_i^3}}{dy^2}\right)_{true} + \cdots, \tag{3.5}$$

$$\overline{u_i^4}_{meas} = \overline{u_i^4}_{true} + \frac{3d^2}{8}\overline{u_i^2}_{true}\left(\frac{d\overline{U}_i}{dy}\right)^2_{true} + \frac{d^2}{4}\left(\frac{d\overline{u_i^3}}{dy}\right)_{true}\left(\frac{d\overline{U}_i}{dy}\right)_{true} + \frac{d^2}{32}\left(\frac{d^2\overline{u_i^4}}{dy^2}\right)_{true} + \cdots. \tag{3.6}$$

In figure 4, data are provided that illustrate the influence of the size of the LDA control volume on turbulence intensity measurements. These data correspond to the measurements of the axial velocity component at $Re = 22100$. As indicated in figure 4(*a*), the dimensions of the LDA control volume appreciably influence the turbulence intensity measurements at moderate and high Reynolds numbers in the region of high shear. Figure 4(*b*) shows the predicted profiles of figure 4(*a*) based on equation (2.4) for correction of turbulence intensity measurements. Both sets of data shown in figure 4(*a,b*) are very similar and confirm that corrections derived are applicable to the measurements taken in turbulent wall shear flows.

To assess further the accuracy of gradient-broadening corrections and the particular choice of a lengthscale d, we shall analyse the limiting behaviour of turbulence intensities near the wall. Since the instantaneous velocity profile of the streamwise velocity component varies in a linear fashion across the viscous sublayer, its RMS ($u' = \overline{u^2}^{1/2}$) value normalized by local mean velocity $\overline{U}$ must approach a constant asymptotic value in this part of the flow. From (3.4) the limiting behaviour of intensity can de deduced as follows:

$$\left(\frac{u'}{\overline{U}}\right)_{meas} = \left[\left(\frac{u'}{\overline{U}}\right)^2_{wall} + \frac{d^2}{16y^2}\right]^{1/2} \quad \text{as} \quad y \to 0. \tag{3.7}$$

Figure 5 shows measured and corrected profiles of $u'/\overline{U}$ close to the wall together with predictions of (3.7). It can be seen that the derived correction works well across the part of the flow where a significant gradient-broadening effect occurs. The measured data closely follow the predicted profile, justifying the choice of a diameter d defined at the e^{-2} light intensity point.

In connection with the issue discussed above, it is interesting to analyse measurements made in a laminar boundary layer developing on a flat plate by Müller (1992). He used a special LDA system and measured the mean velocity and turbulence intensity distributions down to the wall. To verify the reliability of laser-Doppler measurements, complementary investigations were carried out using hot-wire anemometry. To minimize the interaction between the thermal wake from the hot wire and the wall, the test plate was made from Perspex because of its low thermal conductivity. The measured data are shown in figure 6(*a,b*). Whereas the measured mean velocity distributions obtained using two different techniques agree very well with the analytical solution of Blasius (see Schlichting 1968), the profiles of turbulence intensity normalized by the local mean velocity show large discrepancies near the wall. Compared with hot-wire data, turbulence intensities deduced from LDA measurements are higher in the near-wall

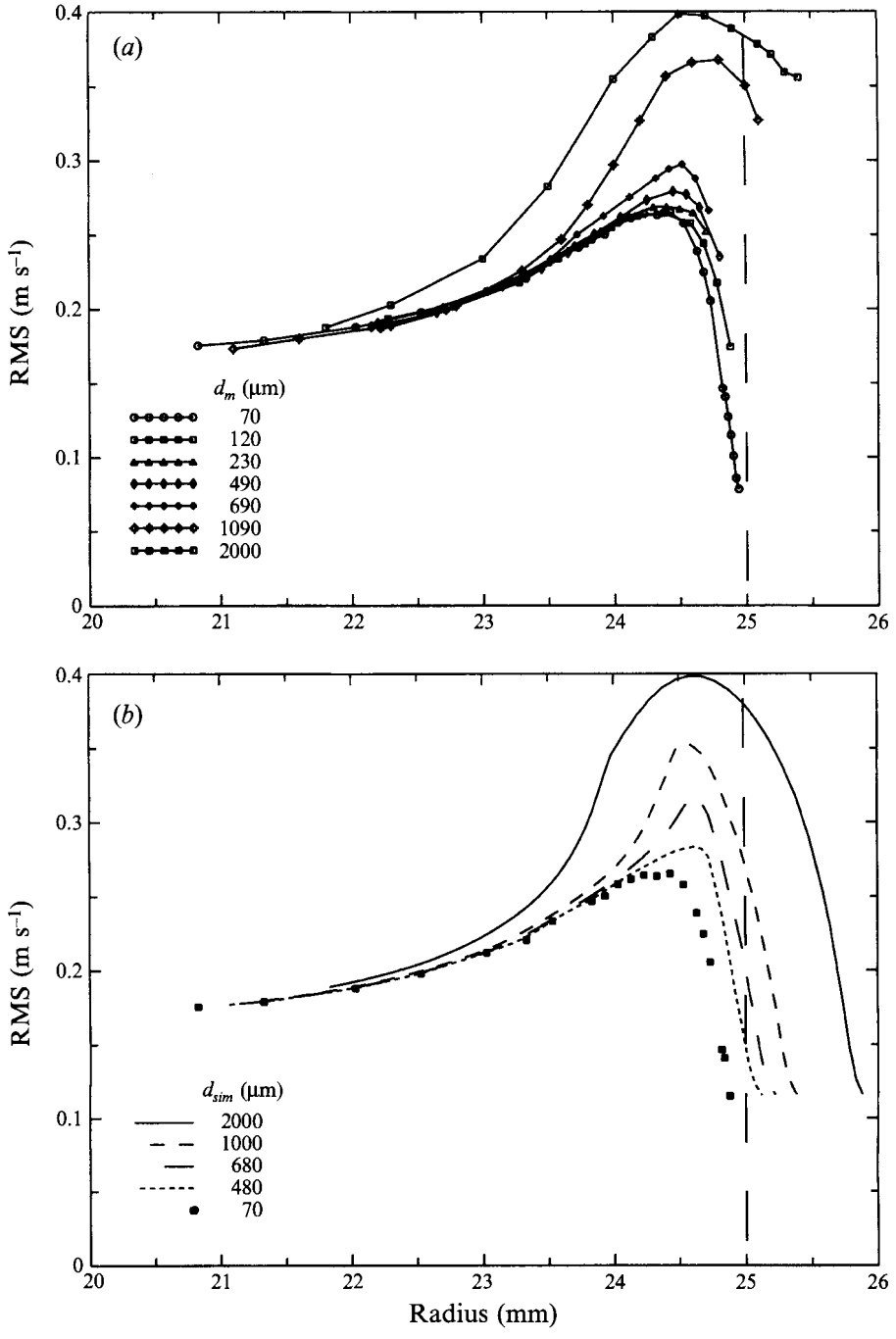

FIGURE 4. Measured and simulated turbulence intensities of the axial velocity component for various diameters of the measuring control volume at $Re = 22\,100$: (*a*) measured; (*b*) simulated.

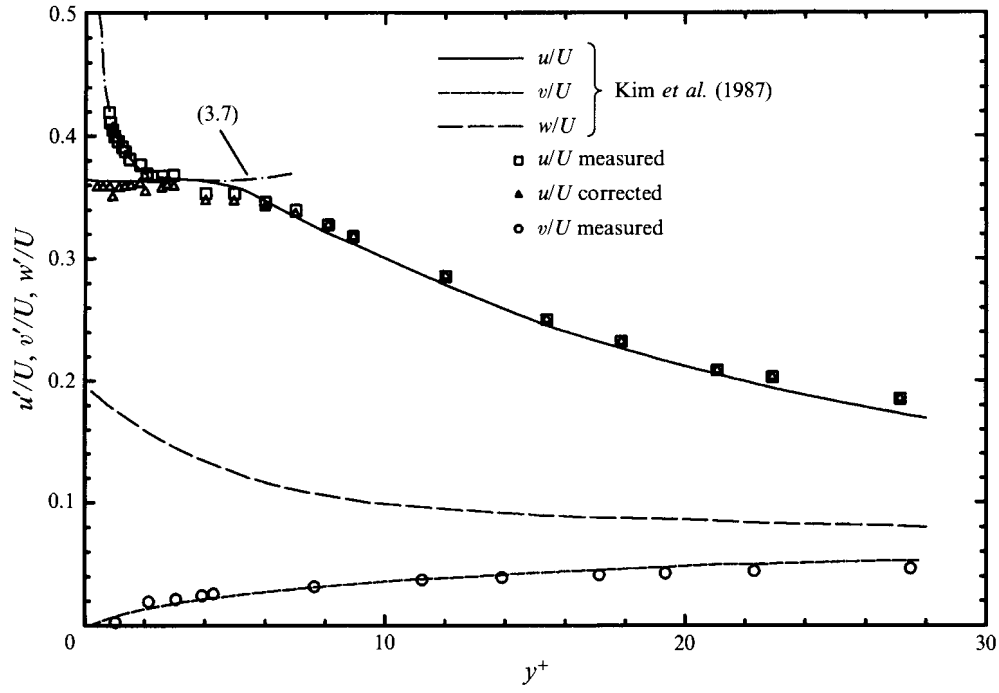

FIGURE 5. Comparison between measured and corrected intensity profiles near the wall.

region. By applying the correction procedure outlined above together with the lengthscale d calculated at the waist of an unfocused laser beam and at the e^{-2} point of the Gaussian light intensity, Müller (1992) was able to match the laser-Doppler and hot-wire results in close proximity to the wall. The results in figure 6(*b*) further demonstrate the ability of the correction procedure used to obtain the limiting behaviour of the turbulence intensity distribution $u'/\overline{U}$ at the wall.

All measurements reported in this paper have been corrected for the influence of the finite size of the LDA measuring control volume using the methodology discussed above. The velocity gradient-broadening corrections were significant only for the axial velocity component in the region of the viscous sublayer.

3.2. *Electronic noise*

The erroneous contributions to LDA frequency measurements, discussed in § 3.1, result from spatial variations of the velocity field yielding Doppler frequency variations across the measuring control volume. In addition to the spatial variations of Doppler frequencies, time variations also contribute to measuring errors. These are mostly caused by electronic noise resulting from the signal processing equipment and/or the electronic drivers of the frequency-shifting units used with the LDA equipment. Contributions of noise of this kind can readily be seen in figure 7, where the raw data of the longitudinal turbulence intensity are plotted, showing a non-vanishing intensity near the wall. This non-zero turbulence intensity remains in spite of the corrections required due to the finite size of the measuring control volume.

An additional noise source should be mentioned for the LDA measurements reported here. It is caused by the light scattered from small impurities collecting on

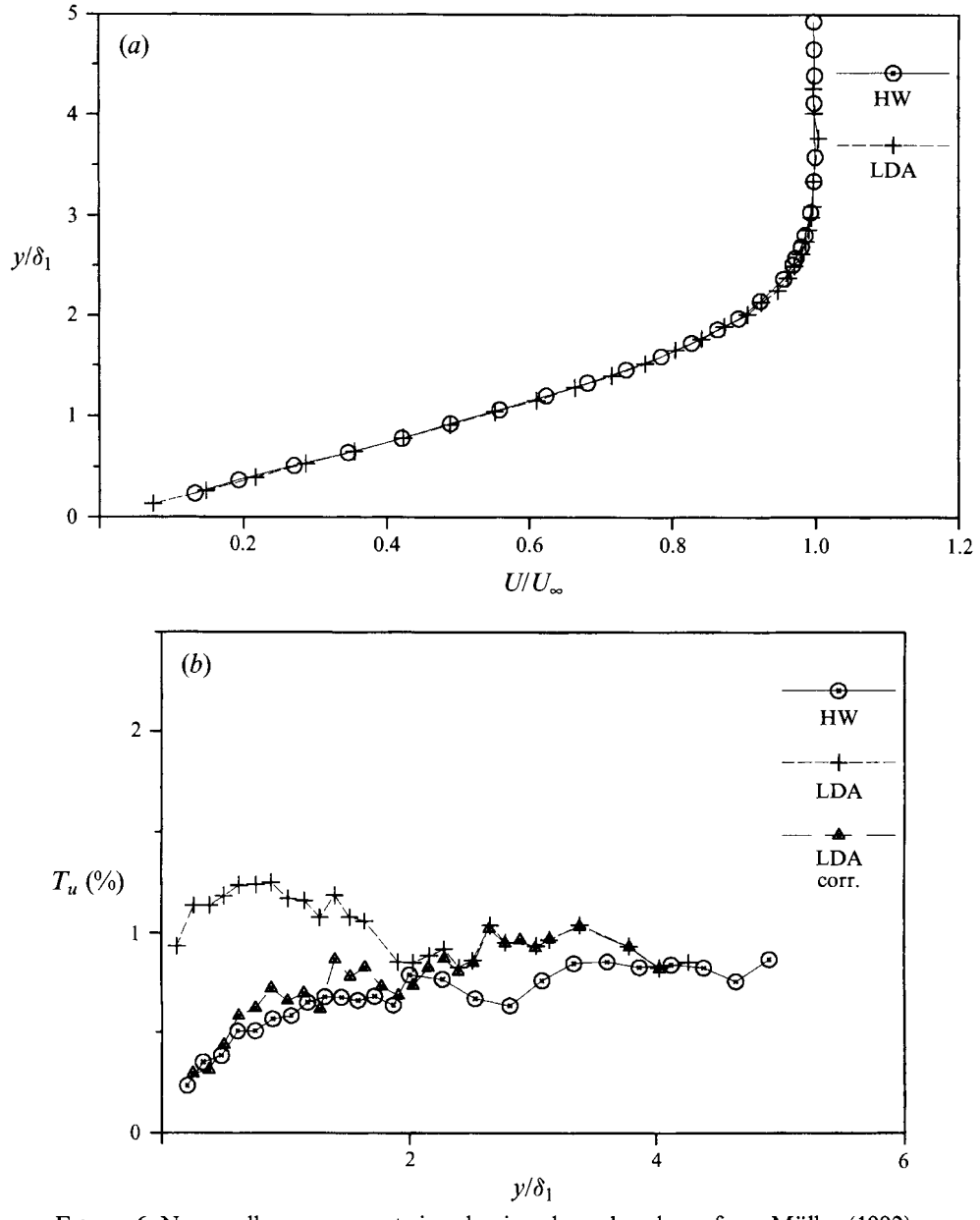

FIGURE 6. Near-wall measurements in a laminar boundary layer from Müller (1992): (*a*) mean velocity profiles; (*b*) turbulence intensity distributions.

the pipe wall, making this wall a highly scattering surface in spite of the matching of the refractive indices of the pipe wall material and the flowing fluid. Hence cleaning the pipe wall prior to the final measurements greatly helps to reduce the noise but, even so, a decreasing signal-to-noise ratio was found as the measuring volume was traversed towards the wall. Detailed studies revealed that a reduction of the frequency shift to 200 kHz and limiting the measurements to distances larger than one half-diameter of the measuring control volume reduced the noise level in all measuring

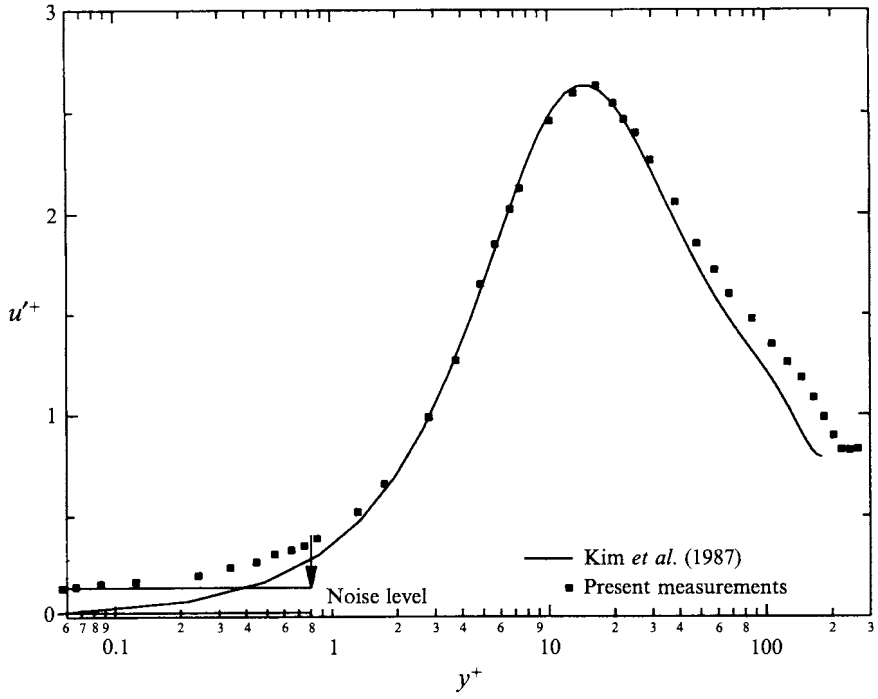

FIGURE 7. Influence of electronic noise on turbulence intensity measurements close to the wall.

points to such a value that no corrections were required. Running the LDA counter processor in its total burst mode also helped to reduce the noise contributions to the flow measurements reported here.

With the application of the correction procedure described in the previous section and by utilizing the results of noise investigations given above, the maximum possible accuracy of measurements was achieved, as demonstrated in figure 8, where the normalized profiles (to be defined later) of mean velocity and turbulence intensity measured at $Re = 7442$ are plotted in the region very close to the wall. Both sets of data exhibit perfect linearity with the coincidence of extrapolated zero locations at the wall surface. With unacceptable noise contributions, a common zero location at the wall is not found. It is interesting that a common zero location at the wall would also not be found if the uniform distribution $F = 1$ was used in (3.1) to correct turbulence intensity measurements close to the wall.

The data in figure 8 are reliable up to the minimum distance from the wall that corresponds approximately to half of the diameter of the LDA measuring control volume. Data closer to the wall could be obtained in the present study, but these contained higher noise contributions.

3.3. *Angle misalignment*

For pipe flow investigations, the accuracy of the measurements also depends on the alignment of the fringe pattern in the measuring volume with respect to the axis of the pipe. If measurements are performed with a single-channel optical system, additional errors can be introduced through the angle of rotation between different readings taken to resolve the velocity components. Recently, Karlsson, Eriksson & Persson (1992) reported that large errors can be introduced into turbulence measurements by

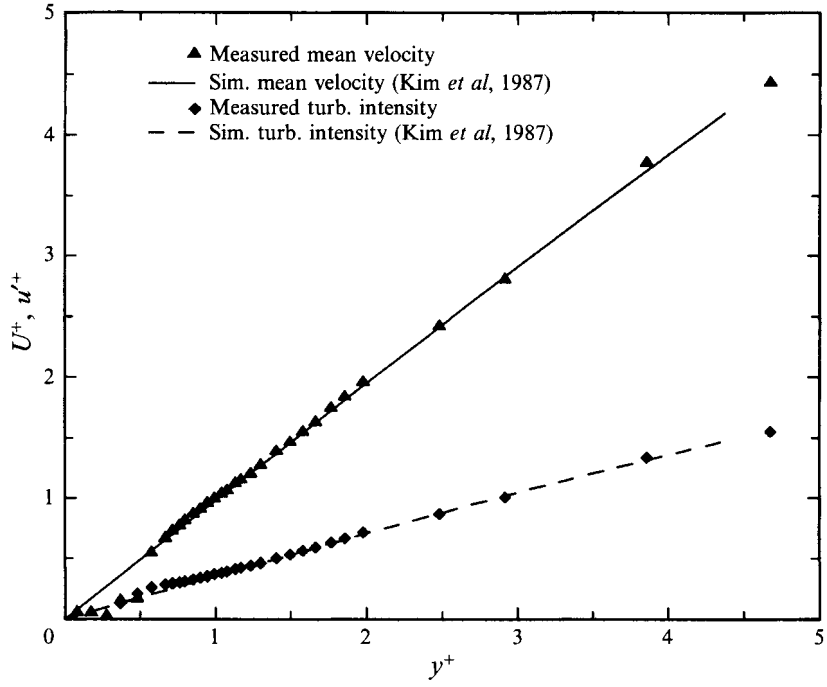

FIGURE 8. Measurements of the mean velocity and turbulence intensity very close to the wall.

laser-Dopler systems by small deviations of the measuring angle with respect to the flow. Their correction procedure was applied to the measured data obtained here. The following strategy was adopted in the measurements.

(i) At each measuring location, the angular error was computed from measured mean velocities in the axial ($\overline{U}_{meas}$) and radial ($\overline{V}_{meas}$) directions:

$$\alpha = \frac{\overline{V}_{meas}}{\overline{U}_{meas} + \overline{V}_{meas}}. \tag{3.8}$$

(ii) It was confirmed, by comparing all angle errors across the entire pipe flow, that the computed α values agreed to within $\pm 2\%$, proving that an angular error really existed.

(iii) An average $\overline{\alpha}$ was applied to correct the measured mean velocity and turbulence intensities as follows:

$$\overline{U} = \frac{\overline{U}_{meas}}{1 - \overline{\alpha}}, \tag{3.9}$$

$$\overline{u^2} = \frac{1}{1 - 2\overline{\alpha}} \left\{ \overline{u^2}_{meas} - 2\overline{\alpha} \left[u_\tau^2 \left(1 - \frac{2y}{D} \right) - \nu \frac{\mathrm{d}\overline{U}}{\mathrm{d}y} \right] \right\}, \tag{3.10}$$

$$\overline{v^2} = \frac{1}{1 - 2\overline{\alpha}} \left\{ \overline{v^2}_{meas} + 2\overline{\alpha} \left[u_\tau^2 \left(1 - \frac{2y}{D} \right) - \nu \frac{\mathrm{d}\overline{U}}{\mathrm{d}y} \right] \right\}. \tag{3.11}$$

Similar corrections can also be derived for the measurements of the tangential component of the velocity fluctuations.

In all cases, the corrections turned out to be negligible when careful initial alignments were carried out. This, in addition, was a good indication of the quality of the test section design and of its careful manufacture.

4. Experimental results

4.1. *Mean flow*

To ensure high statistical reliability of the turbulence measurements, the time interval between samples, Δt, was fixed close to the integral timescale L_τ of the flow (see Lumley 1970):

$$\Delta t \approx L_\tau \approx \frac{D}{\overline{U}_c}, \tag{4.1}$$

where D and $\overline{U}_c$ correspond to the pipe diameter and mean centreline velocity, respectively. Using this sampling time interval, the sample size was set to be $N = 40\,000$, yielding total measuring times of the experiments that were considered to be acceptable. For a sample size of $N = 40\,000$ data points, the relative statistical uncertainty in the measurements could be estimated (on the basis of the sampling parameters, Lumley 1970) to be $\pm 0.28\%$ for the mean velocity, $\pm 1\%$ for the turbulence intensity, and $\pm 2.3\%$ for the fourth-order moment. This statistical reliability was considered sufficient to advance further the present-day knowledge of turbulent pipe flows.

The measured mean velocity, as a function of the normalized distance from the wall, is presented in figure 9. The normalization of measurements was performed with respect to inner wall variables

$$y^+ = \frac{yu_\tau}{\nu} \quad \text{and} \quad U^+ = \frac{\overline{U}}{u_\tau}$$

where u_τ and ν are the wall shear velocity and kinematic viscosity of the flow medium, respectively. The wall shear velocity, u_τ, was calculated directly from the slope of the measured velocity profile in the viscous sublayer. For these purposes, only the data points very close to the wall, i.e. $y^+ \leqslant 2.5$, were considered, as illustrated in the figure 10. This practice ensured accurate determination of wall shear stresses, since the slope of the mean velocity slowly increased as the wall was approached. Only in the region very close to the wall were variations of the shear stress lower than 1%. The value obtained for $Re = 7442$, $u_\tau = 0.043\,\mathrm{m\,s^{-1}}$, was in good agreement with the corresponding value computed from the Blasius equation for the friction factor:

$$\frac{\tau_w}{\frac{1}{2}\rho \overline{U}_B^2} = 0.0791 \left(\frac{\overline{U}_B D}{\nu} \right)^{-1/4}, \tag{4.2}$$

where τ_w is wall shear stress and $\overline{U}_B$ represents bulk velocity.

The measured mean flow distribution shown in figure 9 closely follows the universal law of the wall. The linear and the logarithmic portions of the normalized velocity profile can be easily identified from the measured data. Good agreement of the presented data with the universal law of the wall indicates that the flow had reached a fully developed turbulent state at the location were the flow measurements were carried out.

The two sets of measured data in figure 9 are for the upper and lower halves of the pipe flow, respectively. The data not only agree among themselves, but also show

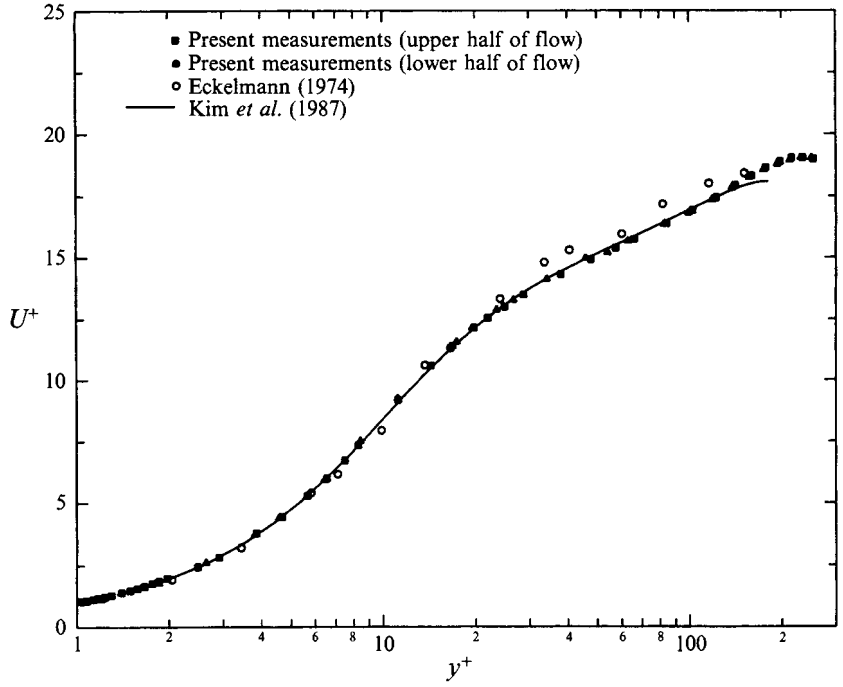

FIGURE 9. Mean velocity distribution for $Re = 7442$.

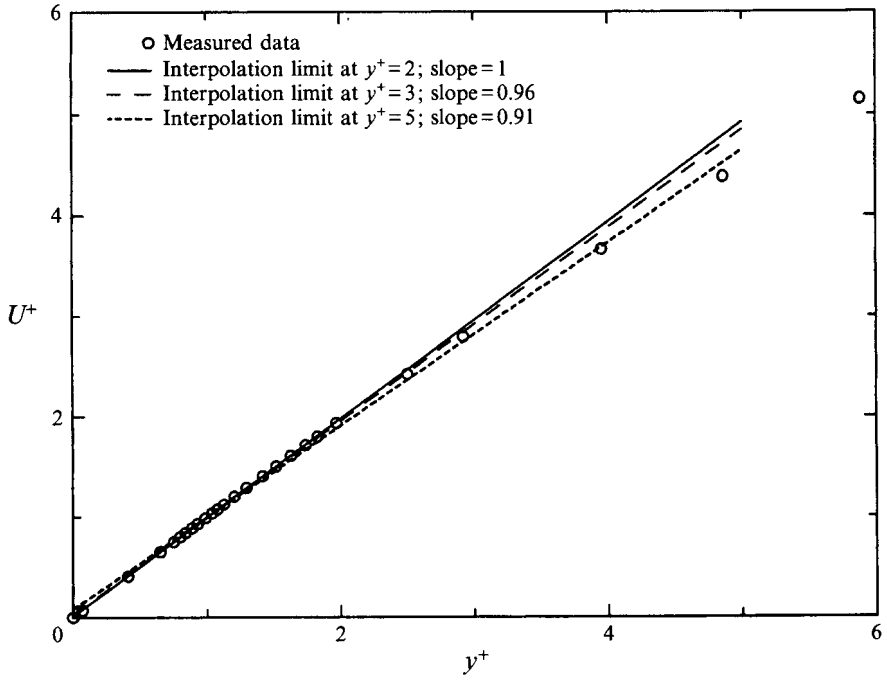

FIGURE 10. Demonstration of different interpolation regions used for wall shear stress measurements.

good agreement with the data from the direct numerical simulations of Kim *et al.* (1987). Although the simulated data correspond to turbulent channel flow, one would expect good agreement across the entire flow field.

4.2. *Turbulence intensity measurements*

Turbulence intensity measurements, normalized with the wall shear velocity, are presented in figure 11. These measurements compare well with the data of Kim *et al.* (1987) across the entire wall region. This can be seen from figure 11 (*a,b,c*), which shows measured RMS values of the axial, radial and tangential velocity fluctuations. Note that the peak in the distribution of the axial intensity is located at the inner edge of the buffer region and that for the distributions of the normal and tangential components at the outer edge. The data in figure 11 also demonstrate some deficiencies in standard hot-wire techniques for near-wall applications. The experimental results of Kreplin & Eckelmann (1979), obtained with an X hot-film probe, show higher intensities in the radial and tangential components of velocity across the entire wall region.

The high reliability of the measured data is further supported by the data shown in figure 12, where the local RMS values of the velocity fluctuations, normalized by the local mean velocity, are plotted in the near-wall region. These data are very sensitive to the accuracy of the measurements of both quantities, since they emphasize the measuring errors that usually increase in the viscous sublayer. The present measurements are nearly identical with the simulated data, supporting the following asymptotic values for the axial and tangential intensities:

$$\frac{\overline{u^2}^{1/2}}{\overline{U}} \approx 0.37, \quad \frac{\overline{w^2}^{1/2}}{\overline{U}} \approx 0.21, \quad y^+ \to 0 \tag{4.3}$$

as the wall is approached. The tangential intensity component is slightly lower than the simulated data close to the wall. This might be related to the limited spatial resolution of the present system for measurements in the tangential direction. The profile of the normal intensity component agrees with the data of numerical simulations down to $y^+ \approx 1$.

In connection with the results presented in figure 12, it is interesting to analyse the limiting behaviour of the turbulence intensities near the wall obtained from various experimental studies. The limiting behaviour of turbulence intensities near the wall reproduced from various experimental studies is given in figure 13 (*a,b*). These data were obtained using different measuring techniques. In general, there seems to be fair agreement among these results for the intensity of the axial velocity component. Hot-wire measurements of Alfredsson *et al.* (1988) and data obtained by Karlsson & Johansson (1986) using laser-Doppler anemometry asymptotically approach slightly higher values ($u'/\bar{U} \approx 0.39$–0.4) than obtained in the present investigations. Good agreement exists between the data shown in figure 12 and the results of Balint, Wallace & Vukoslavčević (1991), Niederschulte, Adrian & Hanratty (1990), Walker & Tiederman 1990 and Wei & Willmarth (1989) away from the viscous sublayer. However, it can be seen from the data shown in figure 13 (*a,b*) that there are significant discrepancies among various experimental results close to the wall.

The data in figure 13 further confirm the shortcomings of conventional hot-wire techniques for near-wall turbulence measurements. The profiles of the axial and tangential intensity components from the study of Kreplin & Eckelmann (1979) are too low compared with the present measurements in the region very close to the wall ($0 < y^+ < 2.5$). The radial component of local turbulence intensity from the same

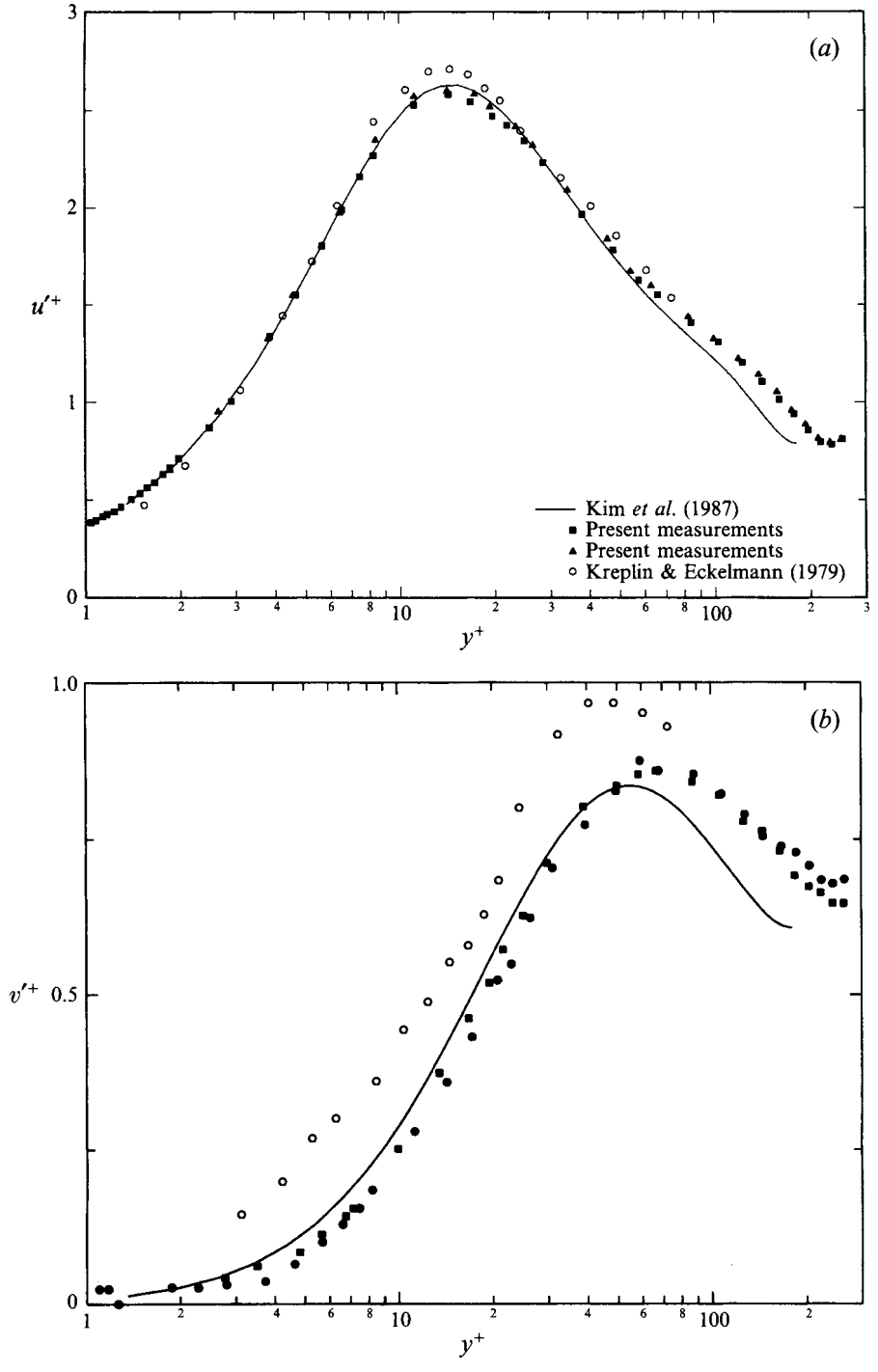

FIGURE 11 (*a*, *b*). For caption see facing page.

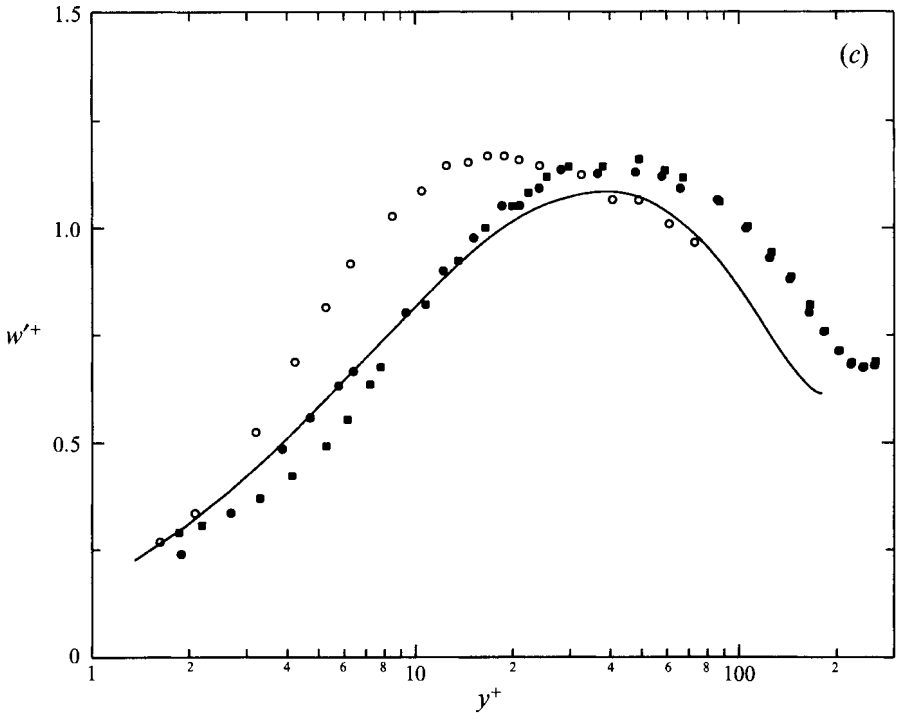

FIGURE 11. Root-mean-square of the velocity fluctuations: (*a*) axial velocity component; (*b*) radial velocity component; (*c*) tangential velocity component.

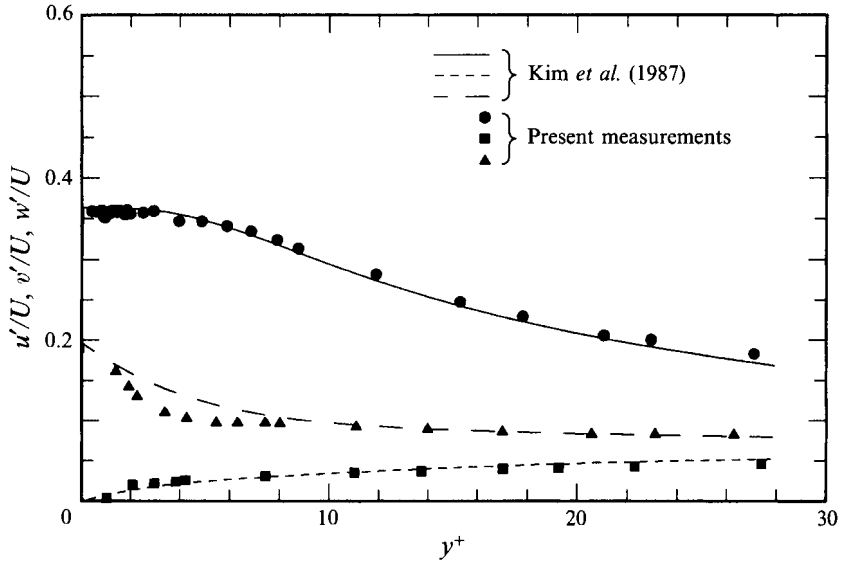

FIGURE 12. Turbulence intensities near the wall normalized by the local mean velocity at $Re = 7442$.

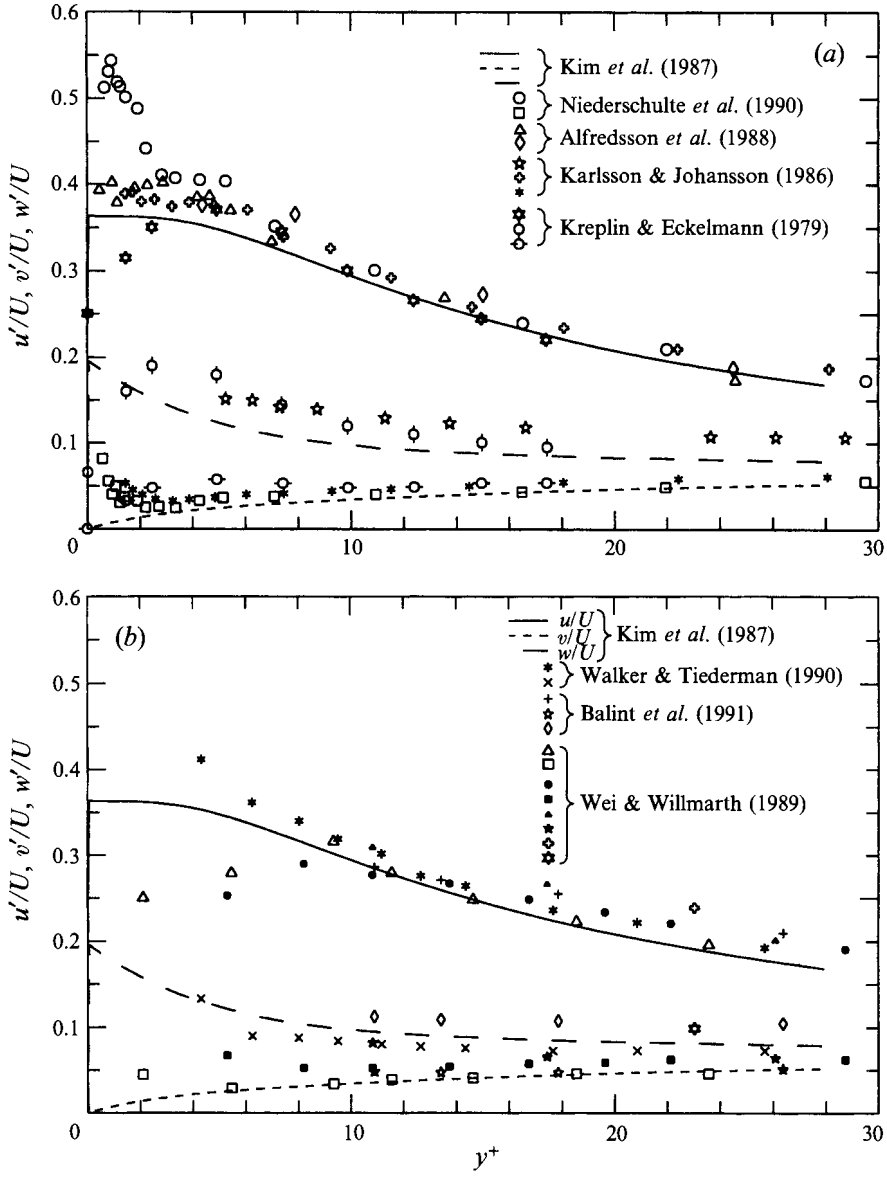

FIGURE 13. Comparison of the limiting behaviour of the turbulence intensities close to the wall reproduced from different experimental studies.

study is nearly double that in the present laser-Doppler measurements in the viscous sublayer.

Since the scatter in the data shown in figure 13 precludes any firm conclusion to be drawn on the scaling of the results presented, an attempt was made to establish the influence of Reynolds number on the limiting behaviour of turbulence intensities near the wall. The data for three different Reynolds numbers, $Re = 7442$, 13 500 and 20 800, are shown in figure 14. These data imply that there is no significant influence of the Reynolds number on the limiting values of turbulence intensities at the solid surface. To further look into this matter, an additional effort was made to measure

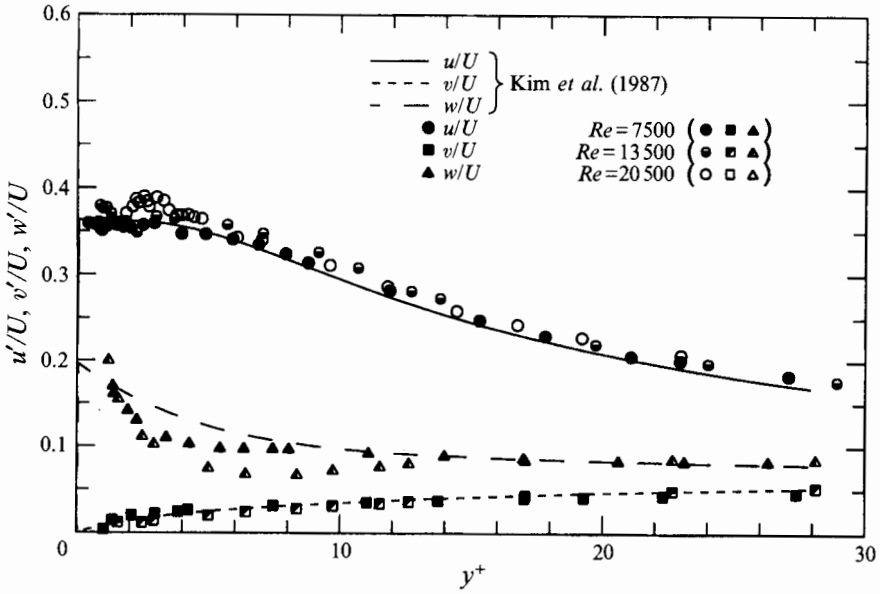

FIGURE 14. Turbulence intensities near the wall normalized by the local mean velocity at different Reynolds numbers.

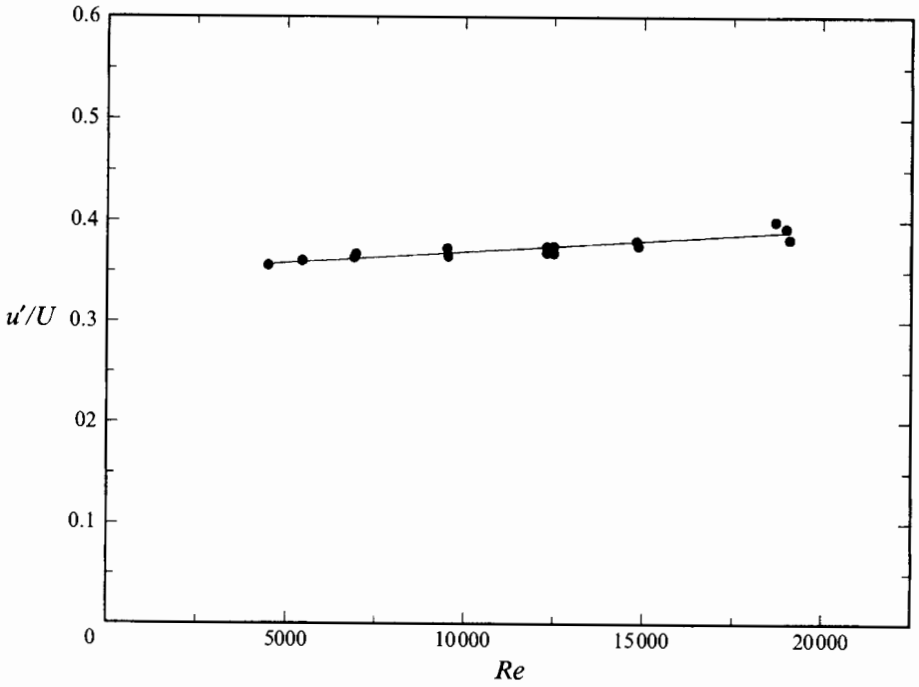

FIGURE 15. Limiting behaviour of the longitudinal turbulence intensity normalized by the local mean velocity at different Reynolds numbers.

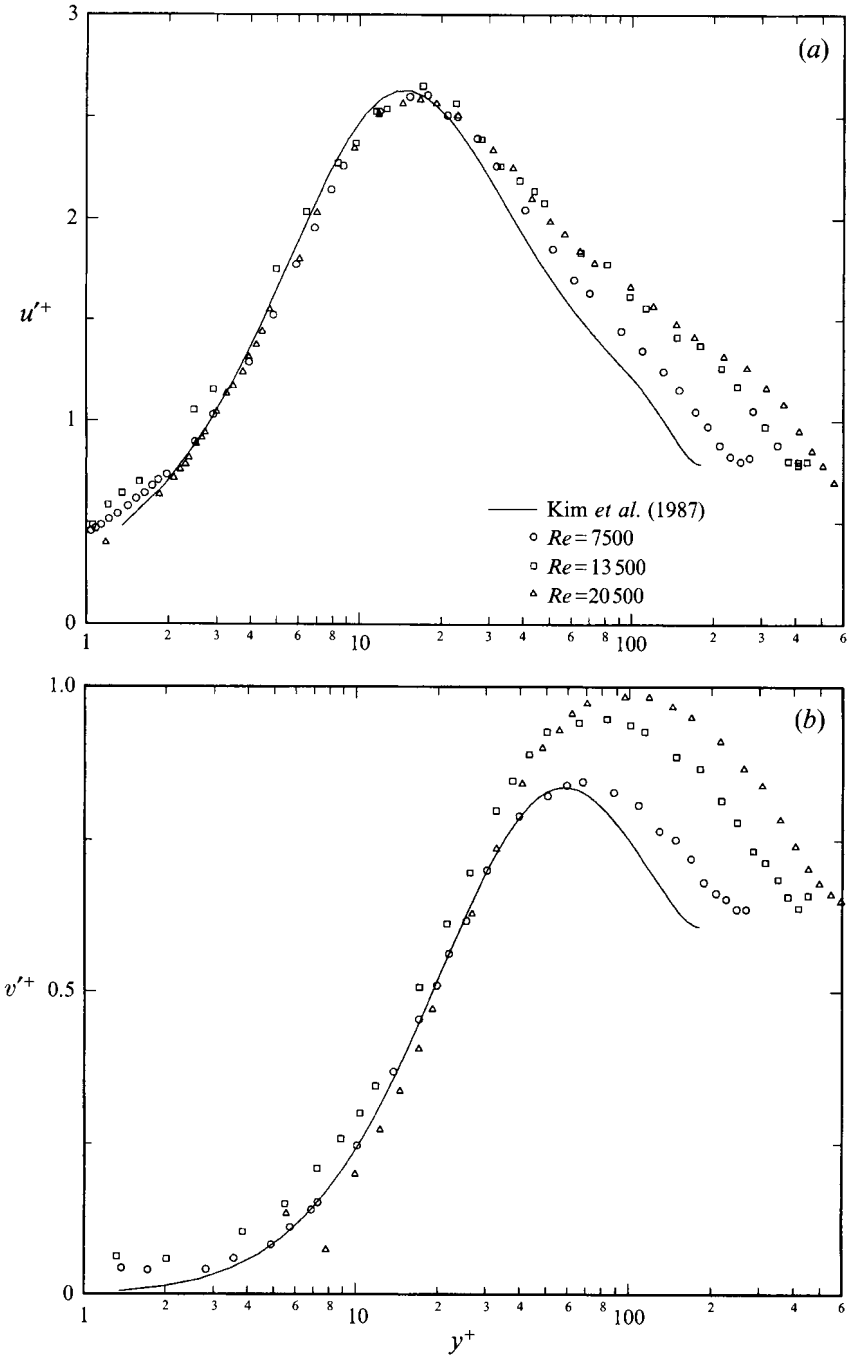

FIGURE 16 (*a*, *b*). For caption see facing page.

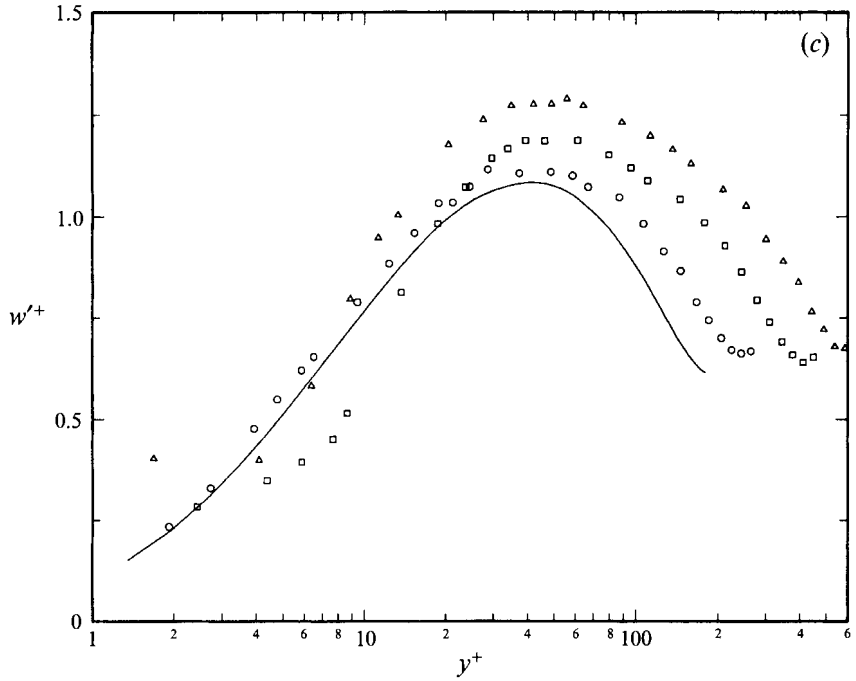

FIGURE 16. Turbulence intensity profiles for different Reynolds numbers: (*a*) streamwise velocity fluctuations; (*b*) radial velocity fluctuations; (*c*) tangential velocity fluctuations.

the limiting behaviour of the axial intensity component

$$\left((\overline{u^2})^{1/2}/\overline{U}\right)_{y\to 0,} \tag{4.4}$$

yielding the results shown in figure 15. Although this figure shows a gentle increase of the limiting value with increasing Reynolds number, this is felt to be partially caused by gradient-broadening effects on the $\overline{u^2}$ measurements. P. Bradshaw (1994, personal communication) pointed out that the trend in the data shown in figure 15 agrees with the limiting behaviour of $u'/\overline{U}$ deduced from direct numerical simulations and therefore cannot be attributed entirely to the instrument response.

Using inner scaling, the dependence of the turbulence intensity components on the Reynolds number is shown in figure 16(*a,b,c*). All sets of presented data displayed in figure 16(*a*) show (within experimental uncertainty) that the streamwise intensity u' scales with the inner variables, starting from the wall up to the point of maximum intensity, located at $y^+ \approx 15$. The peak value of intensity is approximately constant (≈ 2.70) over the Reynolds number range investigated. These findings are in good agreement with experimental observations made in a fully developed turbulent channel flow by Wei & Willmarth (1989) and Antonia *et al.* (1992). Away from the near-wall region, $y^+ \geqslant 15$, the streamwise intensity increases with increasing Reynolds number and decreases less rapidly (with Re) as the centreline of the pipe is approached. Since there is no evidence of a plateau in the u' distribution, we suspect that inner scaling for u' in the logarithmic region can be achieved at much higher Reynolds numbers. The measurements from figure 16(*a*) qualitatively support the ideas of Perry & Abell (1975) about the scaling of fluctuating flow properties in pipe flows. They demonstrated that inner scaling holds for much higher Reynods numbers

(78 000 $\leqslant Re \leqslant$ 260 000) than those attained in the present study. The Reynolds number effects, inferred from figure 16(*a*), are consistent with the trend in the data obtained in the zero-pressure-gradient turbulent boundary layer by Purtell, Klebanoff & Buckley (1981) and Erm, Smits & Joubert (1987).

Using the inner variables, the influence of the Reynolds number on the radial and tangential intensity profiles is shown in figure 16(*b,c*). Within the measuring uncertainty, the v' and w' distributions scale with the wall variables up to $y^+ \approx 20$. For $y^+ \leqslant 20$, v' and w' intensities increase with increase in Re and have a wide peak extending over the entire buffer region. The shapes of these profiles around the points of maximum intensity and the Reynolds number trend are different from the u' distributions. The locations of the maxima for the v' and w' intensities move from the buffer region towards the beginning of the logarithmic region as Re is increased. The above-mentioned variations of turbulence properties with Reynolds number are in close agreement with the measurements of Wei & Willmarth (1989) and Antonia *et al.* (1992) made in a fully developed channel flow.

The experimental results presented have serious implications for the further development of measuring techniques for near-wall studies. The ability of laser-Doppler anemometry to resolve the limiting behaviour of turbulence intensities in the viscous sublayer opens up the possibility of direct measurements of the turbulence dissipation rate at the wall. Such data would be of considerable interest in turbulence research in the near-wall region of pipe and channel flows, since the dissipation rate reaches a maximum value on the solid surface. In this respect, further efforts are needed in order to refine the measurements of the tangential velocity component in the viscous sublayer. Efforts of this kind are in progress.

4.3. *Measurements of higher-order statistics*

During the course of the present investigations, higher-order moments, the skewness and flatness factors of the axial, radial and tangential velocity components, were also measured:

$$S_i = \frac{\overline{u_i^3}}{\overline{u_i^2}^{3/2}}, \qquad F_i = \frac{\overline{u_i^4}}{\overline{u_i^2}^2}, \qquad i = 1, 2, 3. \tag{4.5}$$

These statistical quantities characterize details of the probability density distributions. In wall shear flows, higher-order moments are significantly different from those corresponding to the Gaussian probability function.

The higher-order moments of the axial velocity component are shown in figure 17(*a,b*). The non-Gaussian behaviour of the turbulence fluctuations is mostly localized close to the wall. In the near-wall region, the skewness and flatness factors reach their maximum values:

$$(S_1)_w \approx 0.85, \qquad (F_1)_w \approx 4.1. \tag{4.6}$$

The limiting behaviour of the moments near the wall is in good agreement with the results of direct numerical simulations of channel flow. The present experimental results, numerical data, hot-wire measurements of Alfredsson *et al.* (1988), Kreplin & Eckelmann (1979) and laser-Doppler measurements of Karlsson & Johansson (1986) and Niederschulte *et al.* (1990) compare favourably across the entire wall region.

Whereas there is a fair agreement on the behaviour of higher-order statistics for the axial velocity component obtained from different sources, the same conclusion does not hold for the component perpendicular to the wall. This situation is illustrated in figure 18(*a,b*), where the available skewness and flatness factors are plotted for the

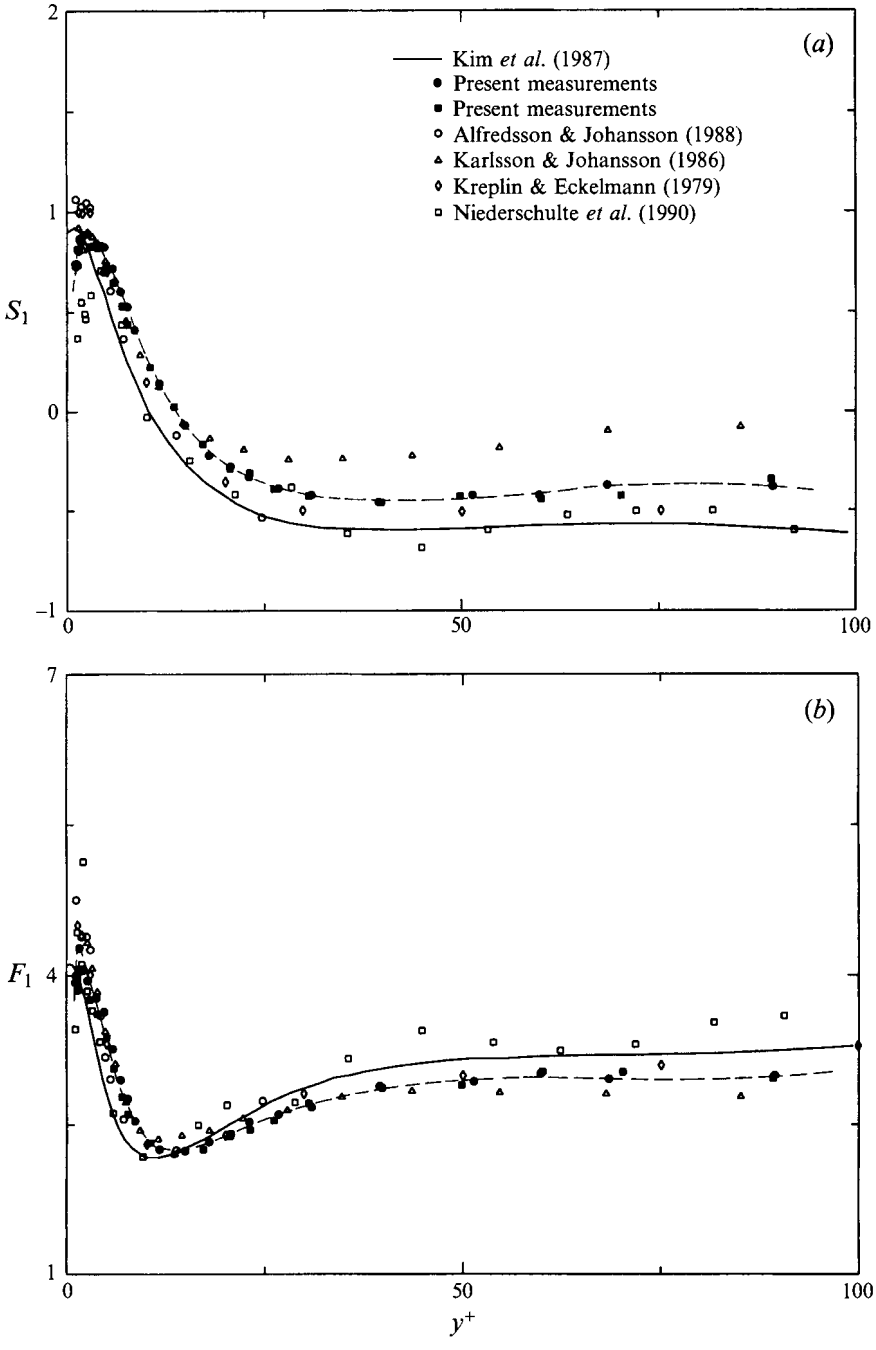

FIGURE 17. Higher-order moments of the axial velocity component: (*a*) skewness factor; (*b*) flatness factor.

radial velocity component. The present measurements of the skewness factor of the v' velocity component agree qualitatively with the simulated data for turbulent channel flow and most of the data obtained from other studies of wall turbulence (Karlsson & Johansson 1986; Niederschulte *et al.* 1990). From the data shown in figure 18(*b*), it is evident that there are noticeable discrepancies between the various results for the flatness factor of the v' velocity component. Whereas the simulated data show a steep rise of the flatness as the wall is approached, the present experiments indicate that the flatness factor reaches a maximum and thereafter decreases towards the wall. Qualitatively, this trend is present in other experimental data obtained using hot-film anemometry (Kreplin & Eckelmann 1979) and laser-Doppler anemometry (Karlsson & Johansson 1986; Niederschulte *et al.* 1990).

It is not clear what the source of the large differences between the experimental and computational data for the flatness factor of v' is, since repeated measurements showed a high reliability of the data in figure 18(*b*). A possible explanation for the strange behaviour of the flatness factor near the wall resulting from numerical computation is given in the recent study of Lyons *et al.* (1991). They analysed the influence of grid resolution on various statistical quantities computed from simulated databases of channel flow. The weak dependence on grid resolution was confirmed for all computed statistics except for the flatness factor of the v' velocity component in the viscous sublayer and buffer region. The flatness factor of the velocity component normal to the wall increased with grid refinement so dramatically that it was not possible to confirm the reliability of this computational result in the entire wall region. Thus, we can conclude that this issue is still open for further investigations.

The distributions of the measured skewness and flatness factors of the tangential velocity components are plotted in figure 19(*a,b*). The skewness is zero across the entire flow field owing to the reflection symmetry, and the measured flatness is in good agreement with the data from numerical simulations. A similar degree of agreement also exists among other available results in the literature (Karlsson & Johansson 1986; Kim *et al.* 1987; Kreplin & Eckelmann 1979; Lyons *et al.* 1991). In the wall region, the flatness factor reaches a maximum value of

$$(F_3)_w \approx 6.75. \tag{4.7}$$

It is interesting to examine the inter-relations between the higher-order moments and turbulence intensity over the cross-section of the pipe. The advanced statistical interpretation of the measurements presented can lead to a class of distribution functions capable of describing non-Gaussian variation of turbulence data. In a recent study, Jovanović, Durst & Johansson (1993) showed that these quantities are highly interconnected, especially close to the wall. They used truncated cumulant expansions as an approximation for the probability density distributions of turbulence quantities together with the basic equations of fluid flow to show that the higher-order moments obey a set of simple differential equations. From these equations, inter-relations between the higher-order moments were deduced that resemble the features of hyperbolic probability density functions. The derived equations also confirmed the well-known fact that the points of maximum turbulence intensity, zero skeweness and minimum flatness factors coincide in the near-wall region.

Figure 20 shows the distributions of the turbulence intensity, skewness and flatness factors of the axial velocity component plotted against the normalized distance from the wall. The increase of the turbulence intensity in the wall region results in a decrease of the non-Gaussian behaviour of the higher-order moments. At the point of maximum intensity, the skewness factor changes sign, and the flatness factor

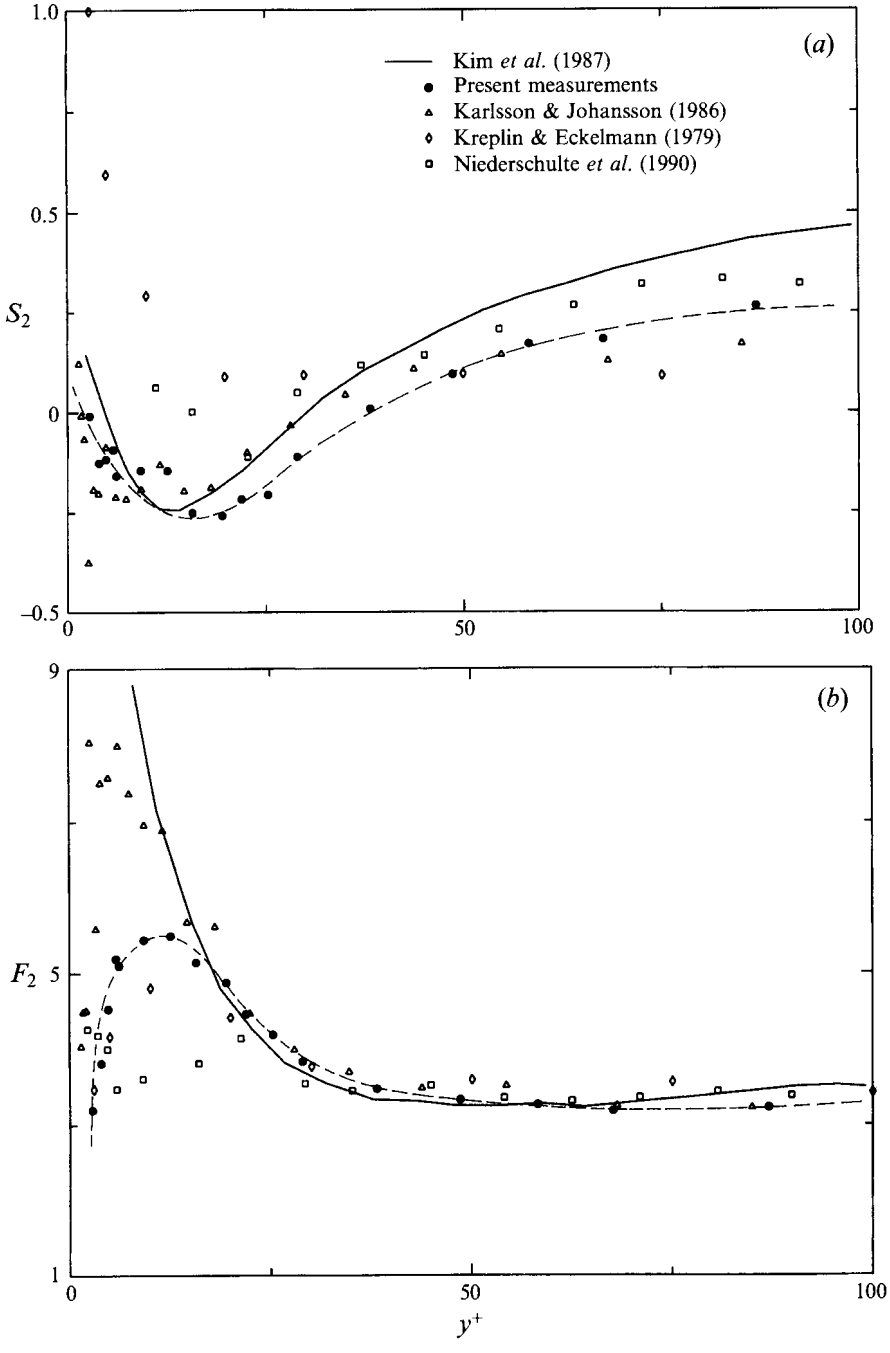

FIGURE 18. Higher-order moments of the radial velocity component: (*a*) skewness factor; (*b*) flatness factor.

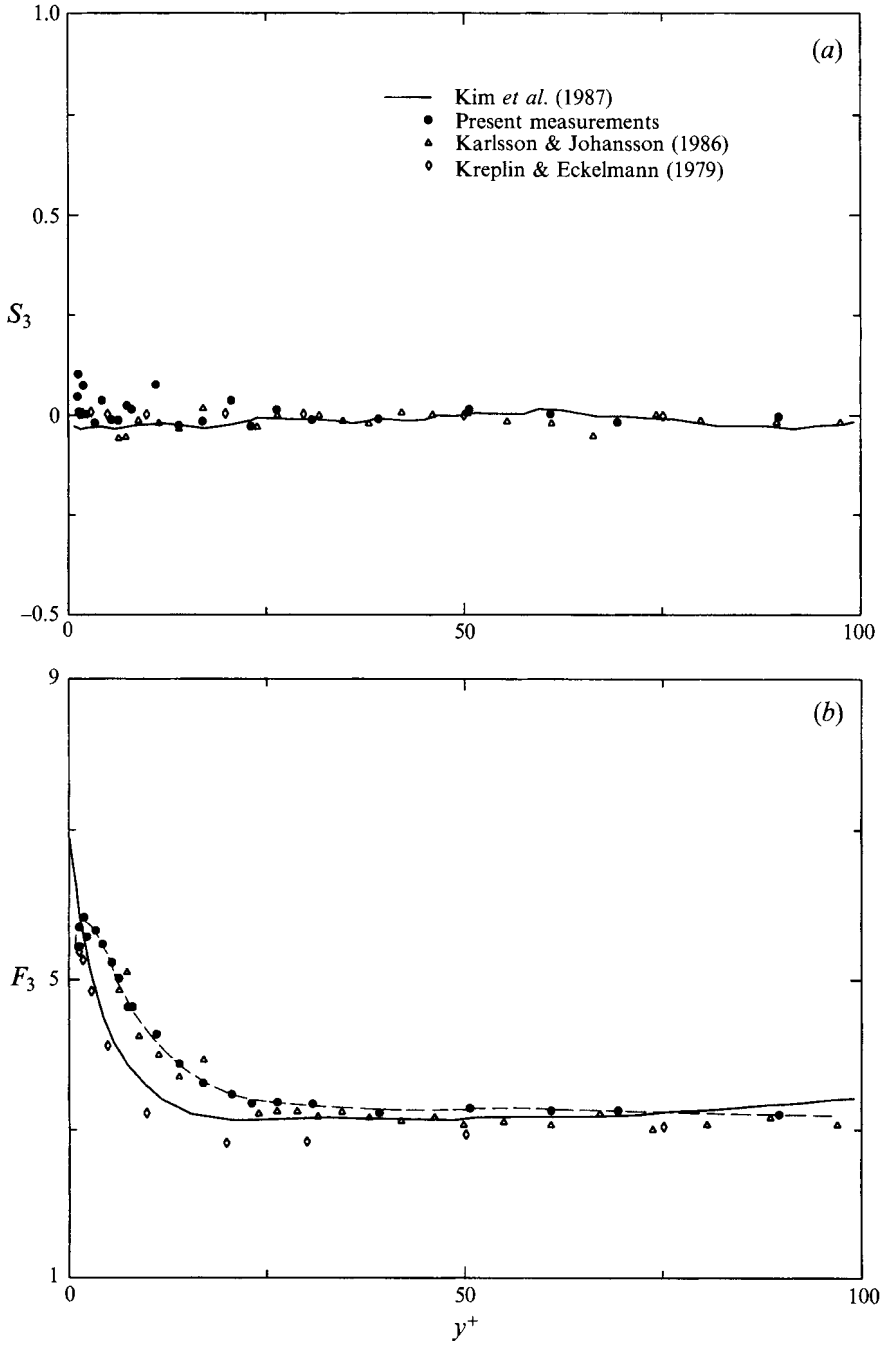

FIGURE 19. Higher-order moments of the tangential velocity components: (*a*) skewness factor; (*b*) flatness factor.

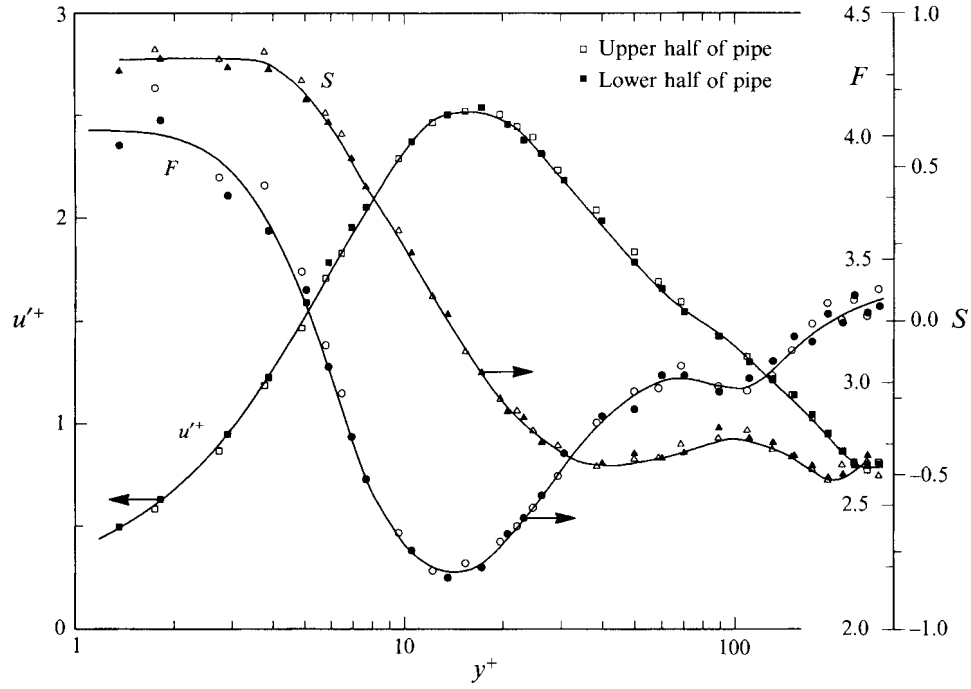

FIGURE 20. Distributions of turbulent intensity, skewness and flatness factors of the axial velocity component.

reaches its minimum value, which is lower than for the Gaussian distribution. The decrease of the intensity away from the wall is associated with a moderate increase of the higher-order moments. The data shown in figure 20 describe the intermodality of the moments in wall shear flows.

5. Conclusions

High-spatial-resolution laser-Doppler measurements have been performed in a pipe flow in order to determine the mean velocity distribution and turbulence statistics in the near-wall region. The experimental results for the mean velocity and turbulence intensities agree well with the results of direct numerical simulations of channel flow down to the minimum distance of $y^+ \approx 0.5$ from the wall. The measured and predicted profiles yield nearly identical data for the limiting behaviour of the turbulence intensities as the wall is approached.

The measured higher-order statistics of the axial and tangential velocity component were found to be consistent with the data obtained from direct numerical simulations including the limiting behaviour of the skewness and flatness factors at the wall. However, significant disagreement was obtained for the higher-order statistics of the cross-flow component. While these two sets of data qualitatively agree for the distribution of the skewness factor, the measured and predicted profiles of flatness completely disagree in the viscous sublayer and buffer region. On the basis of the present measurements it was not possible to clarify the cause of these differences.

Comparisons of the present experimental results with corresponding data from other workers obtained using hot-wire techniques show reasonable agreement for the

statistics of the axial velocity component. The agreement is better away from the wall than in the region of the viscous sublayer. Large discrepancies between the data obtained using different measuring techniques were found for the intensities of the radial and tangential velocity components in the viscous sublayer and buffer region.

Based on the results presented in this paper, the following recommendations can be made for successful laser-Doppler measurements of wall turbulence:

(i) use a refractive-index-matched test section for the flow investigations;

(ii) consider the influence of the finite size of the measuring control volume on the data;

(iii) eliminate or compensate for the noise level in the measured signal (forward scatter, low shift, etc.);

(iv) improve the accuracy of LDA signal evaluations by running the counter processor in the total burst mode;

(v) correct the measurements for the alignment of the fringe pattern in the measuring control volume with respect to the flow;

(vi) to minimize the relative errors in measuring the time averages, do not sample data faster than one integral timescale of the flow;

(vii) check the repeatability of the measurements by performing the same experiments many times.

With the above precautions, it is possible to obtain high-resolution turbulence measurements close to the wall.

REFERENCES

ALFREDSSON, P. H., JOHANSSON, A. V., HARITONIDIS, J. H. & ECKELMANN, H. 1988 The fluctuating wall-shear stress and the velocity field in the viscous sublayer. *Phys. Fluids* **31**, 1026–1033.

ANTONIA, R. A., TEITEL, M., KIM, J. & BROWNE, L. W. B. 1992 Low-Reynolds-number effects in a fully developed turbulent channel flow. *J. Fluid Mech.* **236**, 579–605.

BAKEWELL, H. P. & LUMLEY, J. 1967 Viscous sublayer and adjacent wall region in turbulent pipe flow. *Phys. Fluids* **10**, 1880–1889.

BALINT, J. L., WALLACE, J. M. & VUKOSLAVČEVIĆ, P. 1991 The velocity and vorticity vector fields of a turbulent boundary layer. Part 2. Statistical properties. *J. Fluid Mech.* **228**, 53–86.

DURST, F., MARTINUZZI, R., SENDER, J. & THEVENIN, D. 1992 LDA measurements of mean velocity, RMS value, and higher-order moments of turbulence intensity fluctuations in flow fields with strong velocity gradients. In *Proc. Sixth Intl Symposium on LDA, Lisbon, Portugal*, pp. 5.1.1–5.1.6.

ECKELMANN, H. 1974 The structure of the viscous sublayer and the adjacent wall region in a turbulent channel flow. *J. Fluid Mech.* **65**, 439–459.

ERM, L. P., SMITS, A. J. & JOUBERT, P. N. 1987 Low Reynolds number turbulent boundary layers on a smooth flat surface in a zero pressure gradient. In *Turbulent Shear Flow 5* (ed. F. Durst *et al.*), pp. 186–196. Springer.

GOLDSTEIN, R. J. & ADRIAN, R. J. 1971 Measurements of fluid velocity and gradient using laser-Doppler techniques. *Rev. Sci. Instrum.* **42**, 1317.

JOVANOVIĆ, J. DURST, F. & JOHANSSON, T. G. 1993 Statistical analysis of the dynamic equations for higher-order moments in turbulent wall bounded flows. *Phys. Fluids* A **5**, 2886–2900.

KARLSSON, R. I., ERIKSSON, J. & PERSSON, J. 1992 LDA measurements in a plane wall jet in a large enclosure. *Proc. Sixth Intl Symp. on LDA, Lisbon, Portugal*, pp. 1.5.1–1.5.6.

KARLSSON, R. I. & JOHANSSON, T. G. 1986 LDV measurements of higher-order moments of velocity fluctuations in a boundary layer. In *Laser Anemometry in Fluid Mechanics III* (ed. R.J. Adrian), *Lisbon, Portugal*, pp. 273–289.

KIM, J., MOIN, P. & MOSER, R. 1987 Turbulence statistics in a fully developed channel flow at low Reynolds number. *J. Fluid Mech.* **177**, 133–166.

KREPLIN, H. & ECKELMANN, H. 1979 Behaviour of the three fluctuating velocity components in the wall region. *Phys. Fluids* **22**, 1233–1239.

LUMLEY, J. L. 1970 *Stochastic Tools in Turbulence.* Academic.

LYONS, S. L., HANRATTY, T. J. & MCLAUGHLIN, J. 1991 Large-scale computer simulation of fully developed turbulent channel flow with heat transfer. *Intl J. Numer. Methods Fluids* **13**, 999–1928.

MÜLLER, R. T. 1992 Theoretische und experimentelle Untersuchungen zur Auslegung von Halbleiter-LDAs für Anwendungen in der Aerodynamik. PhD thesis, Universität Erlangen-Nürnberg.

NIEDERSCHULTE, N. A., ADRIAN, R. J. & HANRATTY, T. J. 1990 Measurements of turbulent flow in a channel at low Reynolds numbers. *Exps. Fluids* **9**, 222–230.

PERRY, A. E. ABELL, C. J. 1975 Scaling laws for pipe turbulence. *J. Fluid Mech.* **67**, 257–271.

PURTELL, L. P., KLEBANOFF, P. S. & BUCKLEY, F. T. 1981 Turbulent boundary layer at low Reynolds number. *Phys. Fluids* **24**, 802–811.

SCHLICHTING, H. 1968 *Boundary-Layer Theory*, 6th Edn. McGraw-Hill.

WALKER, D. T. & TIEDERMAN, W. G. 1990 Turbulent structure in a channel flow with polymer injection at the wall. *J. Fluid Mech.* **218**, 377–403.

WEI, T. & WILLMARTH, W.W. 1989 Reynolds-number effects on the structure of a turbulent channel flow. *J. Fluid Mech.* **204**, 57–95.